Engineering the losses and beam divergence in arrays of patch antenna microcavities for terahertz sources

Julien Madéo,[1*] Joel Perez-Urquizo,[1] Yanko Todorov, [2] Carlo Sirtori[2] and Keshav M. Dani[1]

[1]*Femtosecond Spectroscopy Unit, Okinawa Institute of Science and Technology Graduate University, 1919-1 Tancha, Onna, Japan*

[2] *Laboratoire Matériaux et Phénomènes Quantiques, Université Paris Diderot, Sorbonne Paris Cité, CNRS-UMR 7162, 75013 Paris, France*

**julien.madeo@oist.jp*

Abstract: We perform a comprehensive study on the emission from finite arrays of patch antenna microcavities designed for the terahertz range by using a finite element method. The emission properties including quality factors, far-field pattern and photon extraction efficiency are investigated for etched and non-etched structures as a function of the number of resonators, the dielectric layer thickness and period of the array. In addition, the simulations are achieved for lossy and perfect metals and dielectric layers, allowing to extract the radiative and non-radiative contributions to the total quality factors of the arrays. Our study show that this structure can be optimized to obtain low beam divergence (FWHM <10°) and photon extraction efficiencies >50% while keeping a strongly localized mode. These results show that the use of these microcavities would lead to efficient terahertz emitters with a low divergence vertical emission and engineered losses.

Keywords : Terahertz sources, Patch antenna, Microcavity, Arrays, Finite element method

1. Introduction

The use of subwavelength metal-dielectric-metal confinement of an electromagnetic mode has shown to be an efficient way to realize emitters of terahertz radiation. For example, terahertz quantum cascade lasers in metal-metal waveguides [1,2] are demonstrating the highest output powers and heat dissipation but at the cost of a poor beam quality and low photon extraction efficiencies [3]. Multiple photonic structures have been investigated to combine high output power and low beam divergence such as distributed feedback (DFB) [4], horn antennas [5] and antenna-coupled structures [6,7]. An alternative approach is the one based on microcavities which allow deep subwavelength mode confinement and single mode operation [8]. In particular, designs based on patch microcavities have already allowed the demonstration of the ultra-strong coupling regime [9] and strong enhancement of spontaneous emission [10]. This structure confines the mode in a subwavelength dielectric layer between two metallic planes. The resonant frequency is set by making the top metallic layer with a typical length *s* given by $s = \frac{\lambda_0}{2n_{eff}}$, where λ_0 is the free space wavelength and n_{eff} is the mode index. Hybrid structures based on patch antennas have shown to be a promising alternative when used as output couplers [11] or implemented in an external cavity [12]. The use of only patch microcavities in an array could be beneficial to realize efficient terahertz sources but is generally known to output poor beam quality and low photon extraction efficiencies [13,14] due to low radiative losses.

In this work, we use a finite element method to simulate the emission from finite arrays of patch antenna microcavities operating around 3.8 THz. We show that losses, beam divergence and photon extraction efficiencies can be engineered by tuning the number of resonators, their thickness and the period of the array. We show that a beam divergence smaller than 10° (FWHM) can be achieved as well as high photon extraction efficiencies. In addition,

our simulations allow to decouple the radiative and non-radiative contributions to the total losses and show that their relative contributions can be precisely tuned. Our results show that this geometry can be used to achieve terahertz emitters with low beam divergence, single mode operation and high photon out-coupling while keeping a strongly localized mode in the microcavities. In the next section, we will describe the simulation method and model used to investigate the emission of arrays of patch microcavities. Extraction of the studies parameters is illustrated in the case of a single resonator. Section 3 focuses on the quality factors extracted from the simulated emission for various parameters showing that the array geometry allows for higher quality factors than in the single resonator limit. We also discuss the losses and photon extraction efficiencies. Section 4 describes how the beam divergence can be engineered and minimized. Finally, the last section is dedicated to a comparison between etched and non-etched structures and how it impacts on all the above-mentioned features.

2. Simulation method and model

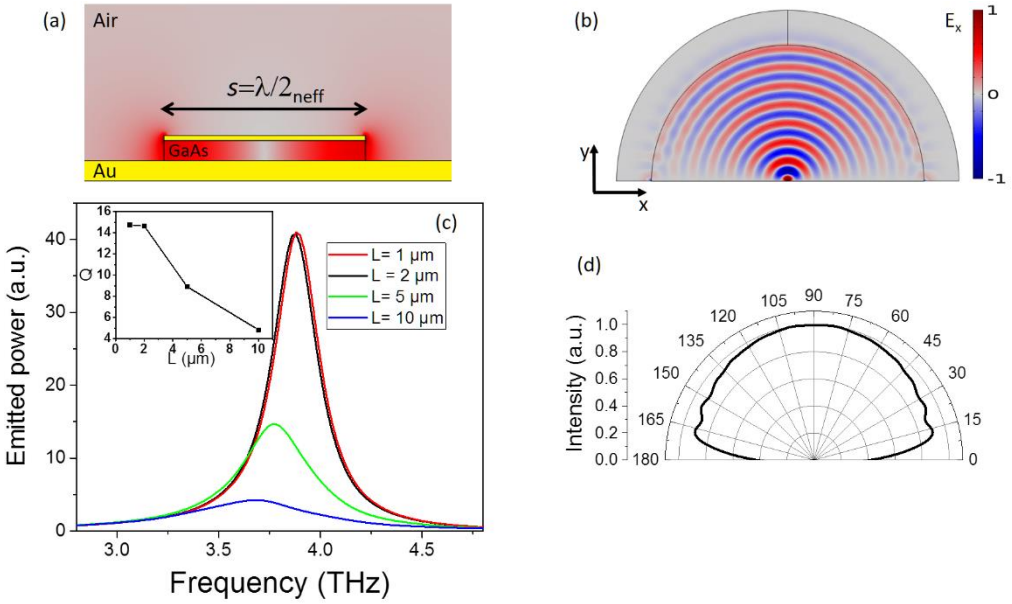

Fig.1 (a) Schematic of a patch microcavity composed of a GaAs layer between a two Au layers. In red is represented the mode intensity. (b)Simulation model showing the radiated field along x direction from a single resonator. The outer parts are perfectly matched layers. (c) Emission spectra for thicknesses of L=1 µm, 2µm, 5µm and 10 µm. Inset: Quality factors obtained from fitting of the simulated spectra with a Lorentzian function. (d) Far-field pattern of a single resonator.

All results presented in the following sections are achieved using a finite element method (Comsol) to study the emission from patch microcavities. All the study is restricted to 2D simulations (1D arrays). This is motivated by: (1) previous work has demonstrated excellent agreement between experimental reflectivity spectra on arrays of square patch microcavities and 2D simulations in the case of infinite arrays [10], (2) 3D simulations of structures including a large quantity of resonators (>100) are time consuming and would require specific High Power Computing resources, and (3) the general trends and underlying physics is similar.

Fig.1(a) presents the design of a patch microcavity. In the rest of this work, *N* defines the number of resonators, the parameter *s* is the length of the resonators (set to 10 µm in all the study), *L* is the dielectric thickness and *d* the distances between two resonators in an array geometry. For the dielectric (metallic) layers, GaAs(Au) is used. Complex refractive indexes were taken from [15] and interpolated. Around the resonance, the input parameters for the complex refractive indices (n+ik) are n_{GaAs}=3.68, k_{GaAs}=0.0044, n_{Au}=188 and k_{Au}=288. An internal source (port 1) in each resonator with a TM polarization is employed to simulate the radiation from the structure. The internal ports are placed at the boundary between the GaAs and the top Au layer. In the case of arrays, the amplitudes and phases of all internal ports are equal. Radiation is then collected in the far-field at the circular boundary (port 2) of an air half disc and a perfectly-matched layer (see Fig.1(b)). The Au ground plane is 1 µm thick and the top metallic layer is 200 nm. The far-field pattern (modulus of the far-field electric component) in Fig.1(d) shows an emission in all directions which does not depends on the dielectric thickness (not shown). To obtain the emission spectra as a function of the frequency υ , we plot $|S_{12}(\upsilon)|^2$. Fig.1(c) presents the emission spectra for a single patch microcavity for dielectric thicknesses of *L*=1 µm, 2 µm, 5 µm and 10 µm. We note that the emission is not renormalized by the thickness as for a terahertz emitter (e.g. quantum cascade structure), the number of emitted photons would depend on the number of periods in the active region. The resonant frequency is redshifted as the thickness increases owing to a lower effective index. Quality factors are extracted from the simulated spectra by using Lorentzian fits (see inset Fig. 1(c)). In the following sections, we discuss the photon extraction efficiencies for various parameters. In general, the different contributions to the total losses are given, in terms of quality factor by the relation:

$$\frac{1}{Q} = \frac{1}{Q_{rad}} + \frac{1}{Q_d} + \frac{1}{Q_m} \qquad (1)$$

where Q is the total quality factor and Q_{rad}, Q_d, Q_m are the quality factors related to the radiative, dielectric and metallic losses, respectively. For simplicity, we set $\frac{1}{Q_d} + \frac{1}{Q_m} = \frac{1}{Q_{nr}}$ with Q_{nr} denoted as non-radiative losses. The photon extraction efficiency η is provided by:

$$\eta = \frac{Q}{Q_{rad}} \quad (2)$$

In order to extract Q_{rad}, simulations are performed by replacing the lossy materials by perfect materials, i.e. replacing the Au metallic planes by a perfect conductor and by setting the imaginary part of the GaAs complex index to 0. Table 1 summarizes the quality factors and extraction efficiencies obtained in the case of single resonators.

Table 1. Quality factors and extraction efficiencies of single patch microcavities

Thickness	Q	Q_{rad}	η
1 µm	14.7	45	0.33
2 µm	14.6	23	0.63

5 µm	8.9	9.4	0.94
10 µm	4.8	4.9	0.98

As expected from this type of resonators, the total quality factors are low [8]. The radiative losses increase with the thickness of the dielectric (smaller mismatch). Interestingly, by varying the thickness, the structure is either dominated by the non-radiative losses (η <0.5) or by radiative losses (η>0.5) and can reach higher extraction efficiencies than in conventional metal-metal planar waveguides for which the facet reflectivity is generally R~0.7-0.9 [16]. This is discussed in more detail in the case of arrays in the next sections.

3. Quality factors and extraction efficiency in arrays of patch microcavities

From this section, we present results obtained on arrays of patch microcavities. A typical radiated field from an array of N=10 resonators and a distance between resonators of d = 30 µm is shown in Fig.2(a). In this section, we focus on the quality factor dependence of the emitted radiation on the number of resonators *N* and distance between resonators *d*. Fig.2(b),(c),(d) show the extracted quality factors with *L*=1 µm, 2 µm and 5 µm for arrays from 2 to 10 resonators compared to the single resonator limit.

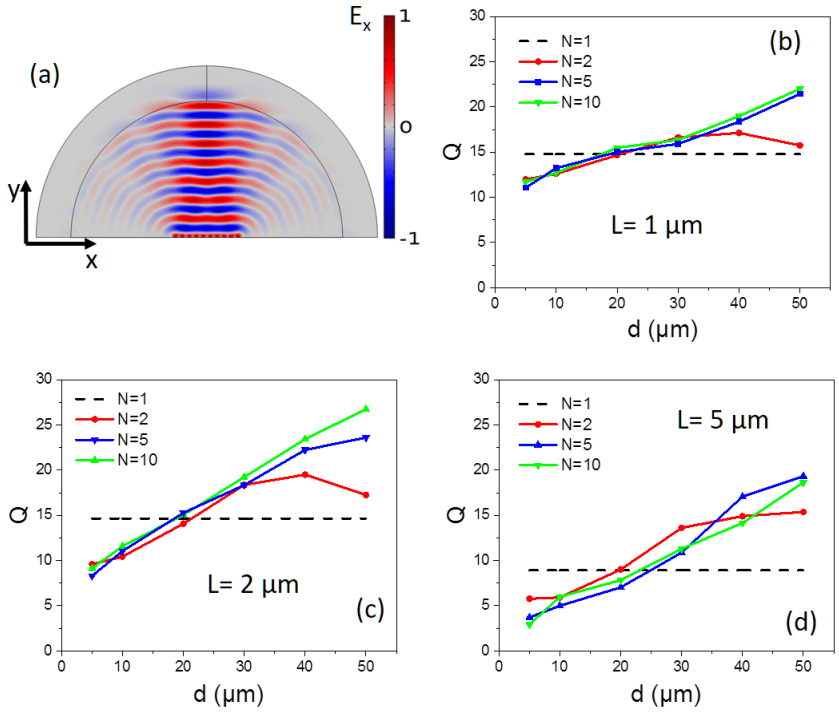

Fig.2. (a) Radiated field from an array of N=10 patch microcavities with d= 30 µm. Quality factors vs distance between resonators d obtained from the simulated emission spectra for N=1,2,5 and 10 and dielectric thicknesses of (b) L=1 µm, (c) L=2 µm and (d) L=5 µm.

For all thicknesses, we observe a similar trend, namely for $d \lesssim 20$ µm, the array quality factors are lower than for a single resonator. This is attributed to coupling between neighboring resonators which broaden the linewidth. For $d \gtrsim 20$ µm, the array geometry provides smaller losses than the single resonator. These results show that in the case of a laser, the period of the array should be large enough to minimize the total losses which would impact directly on the lasing threshold. For the case of a thickness of L=10µm (not shown), the coupling between resonators is stronger due to large radiative losses (see table 1). This leads in a wide and broad linewidths multimode emission for which extracting the quality factors in not accurate. In this case, we estimate that quality factors are lower than 6. The highest quality factor is obtained for a structure with L=2µm because at this thickness the non-radiative and radiative losses are balanced.

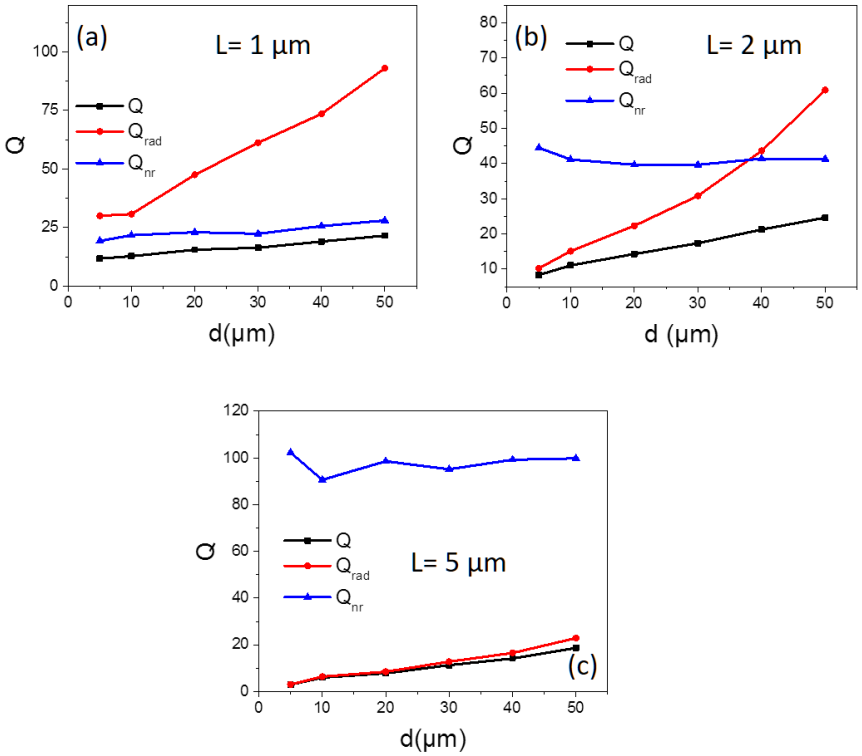

Fig.3 Comparison between total, radiative and non-radiative quality factors vs distance d in the case of N=10 and (a) L=1 µm, (b) L=2 µm and (c) L=5 µm.

Fig.3 displays the total quality factors and the radiative and non-radiative contributions for an array of 10 resonators and L=1 µm, 2µm and 5 µm. We can distinguish three different regimes. For L=1 µm, Q_{rad} is always higher than Q_{nr} so the system is dominated by non-radiative losses. Indeed, in this case the mode is the most confined and thus it has a stronger overlap with the lossy metal. A thickness of L=2 µm corresponds to an intermediate regime for which the two contributions are of similar magnitude. In addition, a perfect balance between radiative and non-radiative can be achieved by tuning the period of the array. For L=5 µm, the system is dominated by its radiative losses. The effect of increasing the period of the array affects only the radiative losses which are reduced as the array is diluted. The non-radiative contributions originate mainly from the dielectric and metallic losses and show no dependence on the distance between resonators. The mode is strongly localized in these microcavities and hence the non-radiative losses are independent of the overall geometry of the array, except in the limit of very dense arrays and/or thick dielectric layers. In Fig.4, we plot the photon extraction efficiency.

Increasing the thickness results in overall higher extraction efficiencies owing to larger radiative losses. As shown previously, the radiative quality factors increase with *d* and become larger than for a single resonator leading in a lower extraction efficiency. We note that for the denser arrays, the photon out-coupling gets higher than for single resonators. Indeed, as mentioned earlier, dense arrays exhibit a coupling between resonators providing a mode delocalized along the structure with larger radiative losses. These results show that very high extraction efficiencies can be obtained. For example, a device with an active region of *L*= 5 µm and an array with *d*= 40 µm has an out-coupling efficiency above 80% which is much higher than what is achieved with metal-metal planar waveguides for which the facet reflectivity is in the range 0.7-0.9 [15] and similar to what can be achieved with DFB structures [17].

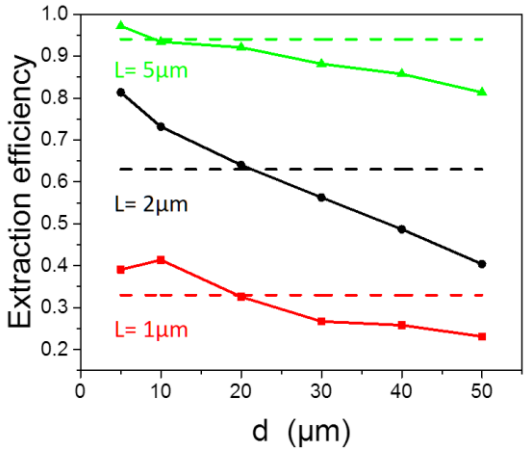

Fig.4 Photon extraction efficiency compared to the single resonator case (dashed lines) in the case of *N*=10 and (a) *L*=1 µm, (b) *L*=2 µm and (c) *L*=5 µm.

4. Beam divergence

The possibility to engineer the directivity of the emission by designing far-field interference is well-known for arrays of patch antennas and is widely used in the RF and microwave bands. Using the fact that the studied microcavities act as patch antennas allow to optimize the beam divergence which makes this design very attractive for multiple applications. The far-field of an array of patch emitters depends on the number of resonators and their spacing. The effect on the far-field from the array parameters can be easily modeled by considering a linear array of *N* point sources separated by a distance *d* interfering in the far-field, the angular dependence on the radiated total power P_{tot} can be simply written [18]:

$$P_{tot}(\varphi) = P_0(\varphi)\left|\frac{\sin(\frac{Nkd\cos(\varphi)}{2})}{N\sin(\frac{kd\cos(\varphi)}{2})}\right|^2 \qquad (3)$$

with φ the angle between the ground plane and the direction of emission and *k* the wavenumber. P_0 corresponds to the radiated power of a single antenna which is assumed to be perfectly

isotropic in our case. This term is modulated by the power gain of the array which is the modulus squared of the quantity known as array factor [18]. It shows that the beam divergence can be reduced by increasing *N* and/or *d*. Fig.5(a) presents the simulated far-field at resonance for *N*=1,2,5,10 and 20 resonators and *d* varied from 5 to 50 µm. As expected, the FWHM divergence improves significantly as the number of resonators and period are increased. For 20 resonators and *d*= 30µm, the FWHM divergence is found to be 9°. Fig.5(c) shows the divergence obtained by using the analytical model provided by equation (3). For d < 10µm, the analytical model underestimates the beam divergence. The effects of near field coupling between the resonators are not included in this calculation which may affect the radiation pattern. For d > 10 µm, the analytical model provides a good agreement with the simulations. We note that simulations predict a saturation of the FWHM divergence whereas the calculation shows a monotonic decrease. For d= 30 µm and N=20, the FWHM divergence is found to be 7°. This simple model provides an easy alternative to estimate the expected far-field from this structure.

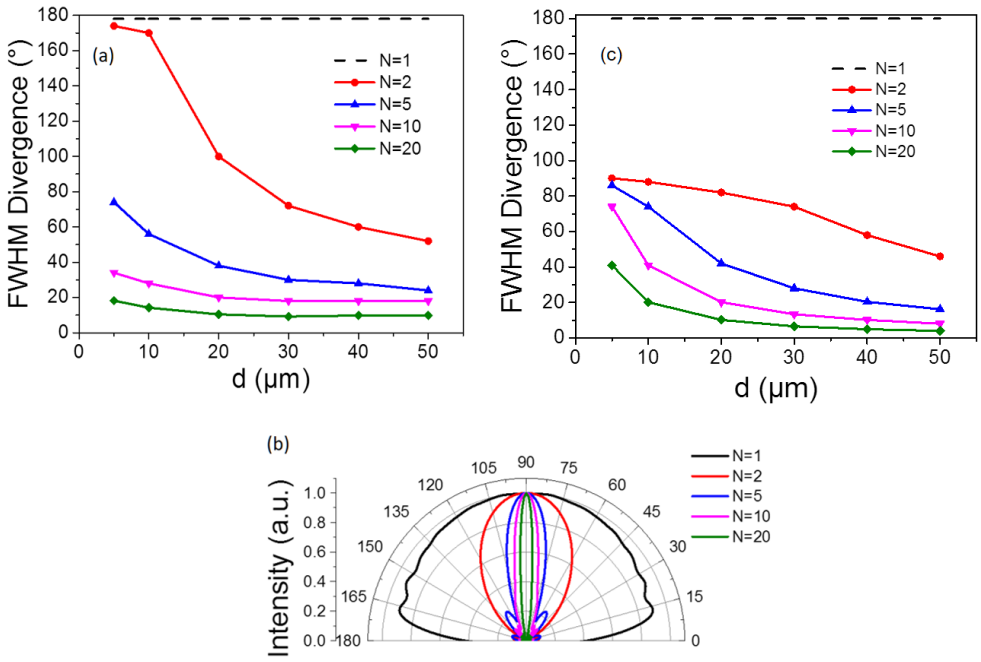

Fig.5 FWHM beam divergence versus distance between resonators *d* for N=1,2,5,10 and 20 simulated by FEM (a) and from the analytical model (c). (b) Far-field patterns for *d* = 30 µm.

5. Etched vs Non-etched structures

Here, we compare the effect of etched and non-etched (only a top metal pattern) structure on the quality factors and far-field pattern. Fig.6(a)(b)(c) summarizes the quality factors of such structure in case of *N*=10. The main effect of a non-etched structure is to reduce confinement. Interestingly, for *L*=1 µm and 2 µm, the quality factors are similar for both etched and unetched

structures. It is only for thicker resonators that there is a there is an advantage of an etched device. Regarding the far-field emission, the beam divergence depends on thickness contrary to etched structures. Whereas the etched structures are showing a saturation above d=30µm, non-etched arrays exhibit a monotonic improvement of the far-field. Above d=40 µm and N=10, a far field smaller than 20° is expected at all considered thicknesses. Regarding the implementation of these geometries for quantum cascade sources, non-etched arrays provides a very simple fabrication process as only a top metallic pattern is needed. However, this solution may add parasitic currents and doped contact layers (not included in this study) may introduce additional losses, reducing the photon out-coupling.

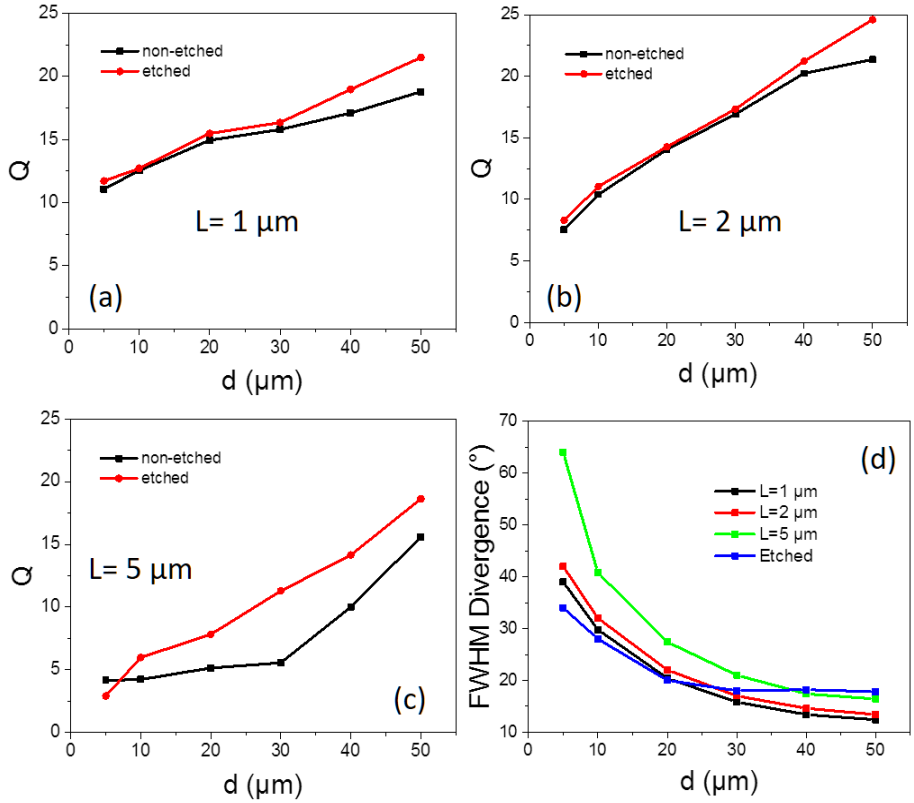

Fig.6 (a)(b)(c) Comparison of quality factors vs distance distance d for N=10 between etched and non-etched structures. (d) Beam divergence vs distance d for various thicknesses of the non-etched structure and for etched structures.

6. Conclusion

By simulating the emission of arrays of patch microcavities, we show that losses and far-field pattern can be engineered by taking advantage of the properties of patch antennas. The quality factors of these structures can be improved by increasing the period of the array. By tuning the thickness, the dominant contribution to the total losses can be selected from non-radiative (thin dielectric layer) to radiative (thick dielectric layer). In addition, diluted arrays and a large number of resonator (>10) lead to improved far-field patterns with a FWHM divergence smaller

than 10°. A comparison between etched and non-etched designs shows that the quality factors are similar for thinner dielectric layers but lower in non-etched structures with thicker dielectric. This study provides results for two-dimensional losses as it is restricted to linear arrays of 2D resonators. When considering 3D resonators, although a similar simulation method with infinite arrays has shown excellent agreement with 2D arrays of square shaped patch microcavities [10], the radiative and non-radiative relative contributions are different [19]. Indeed, the field confinement is stronger leading in weaker radiative losses and higher non-radiative losses owing to a mode confinement in all directions.

Our results show that the use of arrays of patch microcavities can lead to efficient THz sources with a precise control on the losses and the possibility to achieve a narrow beam emission. The implementation of quantum cascade laser active region in such structure would be a simple way to achieve phased array lasers by using the long range coupling of patch antennas, as recently demonstrated in a different type of antenna-coupled design [7]. In a more general manner, our design provides a playground to investigate coherent combinations leading to phase-locked arrays or control of beam divergence and spectral purity [20]. Other possible applications cover surface emitting lasers by implementing THz QCL active region as well as THz amplifiers. In addition, one can take advantage of the strong THz field confinement to enhance nonlinearities for QCLs based on intracavity difference-frequency generation [21].

Acknowledgments

This work was supported by JSPS Kakenhi grant number JP17K14126.

References

1. B. S. Williams, S. Kumar, H. Callebaut, J. L. Reno, Q. Hu, Terahertz quantum-cascade laser at l = 100 μm using metal waveguide for mode confinement, *Applied Physics Letters* **83**, 2124 (2003).
2. B. S. Williams, Terahertz quantum-cascade lasers, Nature Photonics **1**, 517-525 (2007).
3. J. L. Adam, I. Kasalynas, J. N. Hovenier, T. O. Klaassen, E. E. Orlova, B. S. Williams, S. Kumar, Q. Hu, J. L. Reno and J. R. Gao, Beam patterns of terahertz quantum cascade lasers with subwavelength cavity dimensions, *Applied Physics Letters* **88**, 151105 (2006)
4. M. I. Amanti, M. Fischer, G. Scalari, M. Beck and J. Faist, Low-divergence single mode terahertz quantum cascade laser, Nature Photonics **3**, 586-590 (2009).
5. F. Wang, I. Kundu, L. Chen, L. Li, E. H. Linfield, A. G. Davies, S. Moumdji, R. Collombelli, J. Mangeney, J. Tignon and S.S. Dhillon, Engineered far-fields of metal-metal terahertz quantum cascade lasers with integrated planar horn structures, *Optics Express* **24**, 2174-2182 (2016)
6. T.-Y. Kao, X. Cai, A. W. M. Lee, J. L. Reno, Q. Hu, Antenna coupled photonic wire lasers, *Optics Express* **23**, 17091 (2015)
7. T.-Y. Kao, J. L. Reno and Q. Hu, Phase-locked laser arrays through global antenna mutual coupling, *Nature Photonics* **10**, 541-546 (2016).

8. Y. Todorov, L. Tosetto, J. Teissier, A. M. Andrews, P. Klang, R. Colombelli, I. Sagnes, G. Strasser and C. Sirtori, Optical properties of metal-dielectric-metal microcavities in the THz frequency range, *Optics Express* **18**, 13886-13907 (2010).

9. Y. Todorov, A. M. Andrews, R. Colombelli, S. De Liberato, C. Ciuti, P. Klang, G. Strasser and C. Sirtori, Ultrastrong light-matter coupling regime with polariton dots, *Physical Review Letters* **105**, 196402 (2010).

10. J. Madéo, Y. Todorov, A. Gilman, G. Frucci, L. H. Li, A. G. Davies, E. H. Linfield, C. Sirtori and K. M. Dani, Patch antenna microcavity terahertz sources with enhanced emission, *Applied Physics Letters* **109**, 141103 (2016).

11. M. Justen, C. Bonzon, K. Ohtani, M. Beck, U. Graf and J. Faist, 2D patch antenna array on a double metal quantum cascade laser with >90% coupling to a Gaussian beam and selectable facet transparency at 1.9 THz, *Optics Letters* **41**, 4590-4592 (2016)

12. L. Xu, C. A. Curwen, P. W. C. Hon, Q.-S. Chen, T. Itoh and B. S. Williams, Metasurface external cavity laser, *Applied Physics Letters* **107**, 221105 (2015)

13. C. Feuillet-Palma, Y. Todorov, A. Vasanelli and C. Sirtori, Strong near field enhancement in THz nano-antenna arrays, *Scientific Reports* **3**, 1361 (2013)

14. J. Madéo, Y. Todorov and C. Sirtori, Antenna-coupled microcavities for terahertz emission, *Applied Physics Letters* **104**, 031108 (2014)

15. E. D. Palik, Handbook of Optical Constants of Solids, Elsevier (1997)

16. S. Kohen, B. S. Williams and Q. Hu, Electromagnetic modeling of terahertz quantum cascade laser waveguides and resonators, *Journal of Applied Physics* **97**, 053106 (2005)

17. L. Malher, A. Tredicucci, F. Beltram, C. Walther, J. Faist and H. E. Beere, High-power surface emission from terahertz distributed feedback lasers with a dual-slit unit cell, *Applied Physics Letters* **96**, 191109 (2010)

18. R. Mailloux, Phased Array Antenna Handbook, Norwood: Artech House (2005)

19. D. Palaferri, Y. Todorov, A. Mottaghizadeh, G. Frucci, G. Biasiol and C. Sirtori, Ultra-subwavelength resonators for high temperature high performance quantum detectors, *New Journal of Physics* **18**, 113016 (2016)

20. Y. Xie, Y. Li, J. Wang, N. Yang, W. Chu, S. Duan, Power amplification and coherent combination techniques for terahertz quantum cascade lasers, Quantum cascade lasers, Chap.5, Intech (2017)

21. M. A. Belkin, F. Capasso, A. Belyanin, D. L. Sivco, A. Y. Cho, D. C. Oakley, C. J. Vineis, G. W. Turner, Terahertz quantum-cascade-laser source based on intracavity difference-frequency generation, *Nature Photonics* **1**, 288-292 (2007)